Εθνικό Μετσόβιο Πολυτεχνείο
Σχολή Πολιτικών Μηχανικών
Τομέας Γεωτεχνικής

National Technical University of Athens
School of Civil Engineering
Geotechnical Division

Μεταπτυχιακή Εργασία

Κλάδης Αντώνιος

Επιβλέποντες
Καθηγητής Γ. Γκαζέτας

Φεβρουάριος 2016

Αριθμητική Διερεύνηση: Γεφύρας υποβαλλόμενης σε Τεκτονική Διάρρηξη

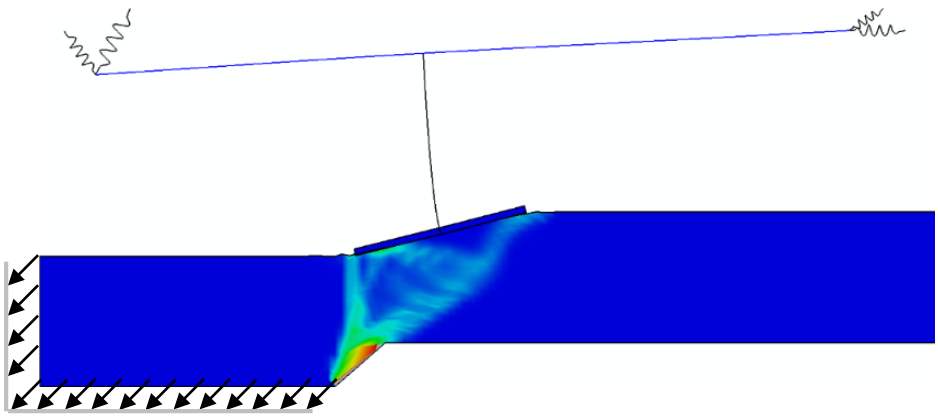

A Numerical Investigation into the mechanics of a Bridge subjected to Surface Fault Rupture

Msc Thesis

Kladis Antonios

Supervisors
Professor G. Gazetas

February 2016

A Numerical Investigation into the mechanics of a Bridge subjected to Surface Fault Rupture

by

A. Kladis, F. Gelagoti, M. Loli, and G. Gazetas

ABSTRACT

Surface fault ruptures may inflict serious damage to bridges built on or near them. In the three notorious earthquakes of Kocaeli, Chi – Chi and Wenchuan a number of bridges were crossed by the emerging normal and thrust faults suffering significant damage, demonstrating, at the same time, the need to account for tectonic deformation in seismic design. Previous research efforts on the subject had been focused on the investigation of the decomposed problem, in which the free-field solution of the fault propagation is preceding the analysis of the bridge system (subjected to the calculated deformations of the free-field step). This paper, attempts a robust investigation of the entire bridge system (soil foundation, pier and deck) with the intention to elucidate the significance (or not) of the kinematic constraints imposed by the superstructure on the overall bridge response. To this end, a typical high-way bridge founded on surface footing is subjected to a dip – slip (normal and thrust) faulting. A series of 1-g physical model experiments are conducted in the split-box of the Soil Mechanics Laboratory of the National Technical University of Athens. In this first part of study, Class-A numerical prediction of forthcoming experimental results is attempted, validating simultaneously the decoupled methodology by *Anastasopoulos et al. 2008*. 2D finite element analyses accounting for soil strain-softening are conducted. The position of the footing relative to the surface fault rupture and the imposed kinematic constraints on the abutments of bridge are also parametrically investigated, assessing the various mechanisms develop and the corresponding stress on bridge.

1. Introduction

In the course of an earthquake, the rupture of the seismogenic fault generates two types of ground displacement: permanent quasi-static offsets on the fault itself, and transient dynamic oscillations away from the fault [*Ambraseys & Jackson, 1984*]. The second type of displacement is the result of waves originating successively from the fault plane and propagating over large distances within the earth crust. Such waves always affect the ground surface and are thus of prime significance for the safety of civil engineering structures. By contrast, the permanent offset of a fault is only evident, when rupture extends all the way to the surface. The latter emerges slowly (as a quasi-static displacement) starting from the bedrock, evolving within the soil deposit to the ground surface, subjecting any structure on its path to extreme movements and sometimes to collapse.

Yet survival is not always impossible. Structures, if design appropriately, may even withstand major fault offsets, due to the favorable interplay of the fault rupture with the structure foundation [*Bray JD. 2001, 2009; Fadaee et al. 2013; Gazetas et al. 2008, 2015*]. The mechanics of such interaction have been thoroughly explored by many researchers [*Oettle & Bray, 2013; Bray & Seed, 1994; Paolucci & Yilmaz, 2008; Anastasopoulos et al. 2008, 2009; Loli et al. 2011*], suggesting that fault rupture may be deviated, protecting structures from unfavorable large tectonic deformations; rigid and continues foundations, of high surcharge were found to perform best under surface faulting.

2. Scope of this study

This paper investigates the response of a bridge system crossed by an emerging fault. Previous studies on the subject propose the use of a two-step decoupled methodology [*Anastasopoulos et al. 2008*]. In the first step the response of a single bridge pier subjected to fault rupture deformation is analyzed, while in the second the detailed model of the superstructure is subjected to the computed, from the previous step, displacements. Therefore, it is inherently assumed that the superstructural system doesn't affect the soil deformations and as such the deformations of the bridge footings. The validity of this assumption will be checked herein by comparing the response of a coupled soil-fault-

foundation-bridge system to the response assessed by applying the decoupled methodology of *Anastasopoulos et al. 2008*.

The problem is studied both experimentally (conducting 1-g experiments at the Fault-Rupture-Box of the National Technical University of Athens), and numerically. This paper presents the results of the numerical investigation.

The structural system of the bridge (i.e. the pier-deck connections and the boundary conditions at the abutments), as well as the fault outcropping position are parametrically investigated. For the sake of brevity, results are presented for the most unfavorable case: the pier is monolithically connected to the deck, and the fault crosses the foundation of the central pier.

3. Problem statement

The investigated problem refers to a typical two-span highway bridge with total length of 34.5 m (Fig. 1). The deck is a hollow section made of pre-stressed concrete, with effective section area of 4.96 m^2 and inertia moment 0.81 m^4. The deck supports a rectangular concrete pier, with dimensions in plain 0.9 x 3.8 m and 8m height. The central pier of bridge is monolithically connected with the bridge deck, while at the two abutments, the deck lies on top of two elastomeric bearings.

The pier is founded through surface footing of prototype dimensions L= 7.5 on top of a sandy stratum.

The bedrock (lying 6 m below the ground surface) is subjected to a 45^o dip-slip angle tectonic dislocation (normal and reverse faulting). The problem is studied both numerically and experimentally and the results are presented in a set of two papers. In this first paper, the numerically methodology is briefly outlined and a class-A prediction of the 1-g experiments is attempted. The experiments have been conducted in the Fault Rupture Box of the NTUA [*Gazetas et al. 2015*], assuming a model scale of 1:15. The dimensions and material properties of the model were scaled down employing appropriate similarity laws [*Muir Wood. 2004*].

4. Bridge subjected to faulting: coupled vs de-coupled analyses

(a) Presentation of the Coupled Methodology

The finite element (FE) method has been applied successfully by several researchers to simulate the fault rupture propagation process in the free-field, as well as the interplay of fault–foundation–structure systems [*Anastasopoulos et al. 2007, 2009; Loli et al. 2011; Bray et al. 1994; Loukidis et al. 2009; Bransby et al. 2008*].

In this study, the soil–foundation-bridge system is analyzed in plane strain conditions. The FE model (Fig. 2) is a numerical replica of the FRB apparatus, and hence its dimensions are equal to those of the split-box in the Laboratory of Soil Mechanics of the National Technical University of Athens. The depth of the soil stratum is 0.40 m (6 m in prototype), while the length is 2.60 m. Note that the length/depth ratio is greater than 4 which minimizes any undesired boundary effect.

Soil and surface footing are simulated with 4-noded plain-strain continuum elements. Following the recommendations of Bray et al (1994), in order to properly simulate the developed shear band, the FE mesh in the neighborhood of the potential rupture should be very refined and a rigorous nonlinear constitutive law for the soil should be assumed. In our numerical model the finite element size is as small as d_{FE} = 0.02 m.

The soil is modelled employing the elastoplastic constitutive model described in [*Anastasopoulos et al. 2007*], and encoded in ABAQUS as a user-defined subroutine. The model incorporates elastic pre-yielding soil behavior, assuming a shear modulus G_S linearly increasing with depth. A Mohr–Coulomb failure criterion is combined with isotropic strain softening, reducing the friction φ and dilation ψ angles with octahedral plastic shear strain γ_{oct}^{pl} according to the following relationships:

$$[\varphi\,;\psi] = \begin{cases} \varphi_\rho - \frac{\varphi_\rho - \varphi_{res}}{\gamma_f^{pl}}\,\gamma_{oct}^{pl}\,;\ \psi_\rho\left(1 - \frac{\gamma_{oct}^{pl}}{\gamma_f^{pl}}\right), & for\ 0 \le \gamma_{oct}^{pl} \le \gamma_f^{pl} \\ \varphi_{res}\,;\,0 & for\ \gamma_{oct}^{pl} \ge \gamma_f^{pl} \end{cases} \quad (1)$$

Where φ_ρ and φ_{res} the peak and residual soil friction angles; ψ_ρ the peak dilation angle; and γ_f^{pl} the octahedral plastic shear strain at the end of softening. Constitutive soil parameters are calibrated on the basis of direct shear tests, and the model has been validated with centrifuge experiments conducted at the University of Dundee, as discussed in detail in [*Anastasopoulos et al. 2007*].

For the small stresses of the reduced-scale experiments presented herein, the mobilized friction angle depends strongly on the stress level. This problem, (which does not exist neither in the centrifuge models, where the stress level is equivalent to the prototype thanks to the centrifugal acceleration which multiplies the gravitational force by a factor of N (i.e., equal to the scale of the model), nor in reality), is known as scale effects. To account scale effects in the numerical modelling, φ and ψ are being iteratively adjusted (according to Eq. 1) to be always consistent with γ_f^{pl} and σ_{oct} (octahedral stress).

The fault offset is simulated as a monotonically increasing displacement at the model base. The bottom boundary is divided into two parts; one part (right) remains stationary (representing the footwall), and the other (left) block moves up or down to simulate normal or reverse faulting, respectively. After imposing the geostatic stresses and the dead load of the superstructure, the fault dislocation is applied in small quasi-static analysis increments.

The pier and the deck are modeled with 2-noded beam elements, while the bearings of each abutment are modelled using special 2-noded elastic spring elements of horizontal stiffness K_H=3846 kN/m and rotational stiffness K_R=22222 kNm/rad. The vertical stiffness of the abutments is extremely high and therefore zero vertical displacement has been prescribed.

The soil-footing interface is modelled using special contact elements that allow sliding, uplifting and / or separation (loss of contact). In the experiments, sandpaper are glued on the bottom of footing to increase the interface friction to realistic levels. Thus, a friction coefficient of $\mu = 0.7$ is an appropriate value for the interface between sand and sandpaper.

The bridge deck is modeled as a linearly elastic (assuming that the expected bending moment would be much lower than the bending capacity of this massive deck). The pier, on the other hand is simulated assuming a non- sectional moment (**M**) -curvature (**1/r**) (as

portrayed in Fig. 3). The ultimate value of pier moment is M_{ult}=6500 kNm, equivalent with 0.13 kNm in model scale units.

The backfill consists of dry ‘‘Longstone’’ sand, a very fine uniform quartz sand with d_{50}= 0.15 mm and uniformity coefficient $C_u = D_{60}/D_{10} \approx 1.4$, industrially produced with adequate quality control. The void ratios at the loosest and densest state were measured as $e_{max} = 0.995$ and $e_{min} = 0.614$, while $G_s = 2.64$. Direct shear tests have been carried out to obtain the peak and post-peak strength characteristics of the sand. Medium loose [$D_r = (45 \pm 2$ %)] and dense [$D_r = (80 \pm 3$ %)] sand specimens were tested at normal stresses ranging from 13 kPa (due to the weight of the top cap only) to 300kPa, while the correspondent soil data for medium dense sand [$D_r = (60 \pm 2$ %)] was proceeded with linear extrapolation. As documented in [*Anastasopoulos et al. 2010*], the angle of shearing resistance depends strongly on the stress level; for stresses higher than 120 kPa, referring to loose sand, $\phi' = 32^o$ while for lower stresses ϕ' increases up to 45^o. For the dense specimens the angle of shearing resistance is 35^o for the higher stress levels and 51^o at the lowest normal stress tested. For the soil of this study [$D_r = (60 \pm 2$ %)], the distribution of ϕ' in function with specimen vertical stress (σ) is shown in Fig. 4. These values drop after displacement of 6 mm to post-peak critical-state. The angle of dilation also depends on the effective stress [Bolton. 1986], with a maximum value $\psi = 12^o$.

(b) The Decoupled Methodology

To rigorously assess the performance of a structure undergoing large tectonic deformation, the analysis of the entire soil-fault-structure system is required (Fig. 2). Yet this type of analysis (the attributes of which were systematically presented in the previous paragraph) is all but simple. To overcome this obstacle *Anastasopoulos et al. 2008* proposed a simplified methodology to be used in the design of bridges against faulting.

The problem is decoupled in two subsequent analysis steps. In the first step, the response of a single pier and its foundation to fault rupture propagating through the soil is modeled (local model), while the superstructure is introduced in a simplified manner. In particular, as schematically portrayed in Fig.5 the local model should include: the soil model, the foundation, and the bridge-pier of height H_p and stiffness EI_p, while the bridge deck is replaced by equivalent lateral and rotational springs, K_x and K_θ, respectively. For the case of a continuous deck monolithically connected to piers, K_x represents the axial stiffness of the deck and K_θ the bending stiffness of the pier-deck connection. Correspondingly, for a seismically isolated bridge, K_x and K_θ represent the lateral and rotational stiffness of the (elastomeric) bearings. In our study, however, the pier is monolithically connected with deck and (elastomeric) bearings are placed on the edges of model. For this reason, the axial stiffness of deck K_x is substituted with the horizontal stiffness of bearings, while the rotational stiffness K_θ, is equal with the bending stiffness of the pier-deck connection. This step provides the horizontal (Δx) and vertical (Δy) displacements and the rotation θ at the base of pier that are necessary for the next step.

In the second Step the detailed model of the superstructure (global model) is analyzed, subjected to the support (differential) displacements estimated in the previous step. Since this work was part of a research project in Greece, emphasis had placed on normal faulting (the dominant mode in Greece), however, in this study is applied both normal and reverse faults.

This paper attempts a forward comparison between the coupled and the de-coupled type of analysis for a bridge system experiencing normal or reverse faulting. The comparison will be provided in terms of settlement and rotation at bridge-footing, bending stress on the pier and the deck of bridge, as well.

5. Results: Bridge subjected to Normal Faulting

The example bridge of Fig. 2 is subjected to normal faulting and its response is assessed utilizing both the coupled and the decoupled methodology. Fig. 6(a) compares the bending stress for the two bridge piers. Evidently, both analyses results are in a very similar pier response. Failure occurs first at the base of the pier, followed by a rapid increase in the bending stressing at the top of pier (pier-deck connection). Yet, the decoupled system fails first (at δ/δ_{max} = 0.27), compared to the coupled system where failure is expected for a higher fault dislocation (i.e. δ/δ_{max} =0.33).

The paradox in this behavior is that the onset of failure in the two piers is different, although the both of them are experiencing identical footing rotations.

As explained by the sketch of Fig. 6(c), both systems develop positive footing rotations, which are inducing positive curvature on the pier-base. Yet, as explained previously, the coupled system is further distressed by the imposed displacements at the left bridge abutment. The latter are displacing the top of the pier to the left introducing a negative curvature on the pier base, practically relieving the pier from the bending stress introduced by the foundation rotation. This explains the broader margins of safety introduced by the coupled analysis.

Fig. 7(a) compares the settlement and rotation of the footing of the two types of analyses. The results are very close: the footing in both analyses performs in a quite similar manner. What is interesting to note is the non-smooth evolution of foundation deformation of the decoupled system at δ/δ_{max} = 0.30. A schematic explanation of this peculiar behavior is portrayed in Fig. 7(b). Initially (for δ/δ_{max}<0.30), as the hanging wall movement increases, a clear gap at the left corner of footing is appearing. This gap rapidly closes at δ/δ_{max} = 0.30 when a plastic hinge at the base of the pier (δ/δ_{max} = 0.27) has been fully formed. At that instant the superstructure is unable to resist to the imposed deformations and abruptly (evidenced by the step-like pattern of the plots at that particular instant) follows the soil deformations.

The differences are much more pronounced in terms of drift ratio presented in Fig. 8(a). For δ values lower than δ/δ_{max} = 0.27 (i.e. before the plastic hinging of pier), both systems

develop positive drift ratios as a result of the left rotation of the footing. Of course, it is no surprise that at any point of this stage, the drift accumulated by the coupled system is much higher. In the latter, fault dislocations are simultaneously imposed to the bedrock (base of model) and to the left abutment of bridge (lying on the hanging wall) dragging the bridge pier farther to the left, whilst in the decoupled system the drift is resulted by bedrock dislocations only. After the plastification of pier the trend changes completely: the coupled system keeps accumulating positive drifts while the decoupled system provokes negative drifts. A view of the deformed mesh at time-step δ/δ_{max} = 0.8 is illustrated in Fig. 8(b), to assist the interpretation of this behavior. After the plastification of pier (δ/δ_{max} = 0.27) the increase of rotation does not affect the horizontal movement of its top, but plasticize more its base, as shown schematically in Fig. 8(c) for the case of decoupled system. As a result only the base of pier moves to the left, leaving the top back and making the drift negative. The difference of coupled system is that fault dislocations are simultaneously imposed to the bedrock and to the left abutment of bridge, as previously mentioned, dragging the top of the pier farther to the left, remaining the drift positive.

The distribution of bending moments across the deck of bridge, for imposed fault dislocation (δ/δ_{max} = 0.35), is presented in Fig. 9(a). As we can observe, the distribution makes a discontinuity in the place of pier. This jump is equal with the bending moment on top of the pier, as it is obliged from node equilibrium. For the same dislocation level, a comparison between the coupled and decoupled system in terms of bending moments across the deck is presented in Fig. 9(b). The evolution of settlement, rotation and horizontal displacement of footing (the output of decoupled pier model) is used as input fault dislocations on the base of pier of decoupled detailed model. As a result the discrepancies between the coupled and decoupled b model, are caused by their discrepancies in terms of settlement and rotation of footing.

6. Results: Bridge subjected to Reverse Faulting

In this section two reverse fault scenarios are examined. In the first scenario the free-field rupture crosses the bridge footing near to its right corner (s/B=0.11), causing maximum displacements on the basis of pier, while in the second one the free-field rupture crosses the bridge footing near to its center (s/B=0.46). Both cases are schematically illustrated in Fig. 10.

Location 1: s/B = 0.11

As evidenced by the plots of Fig. 11(a), and contrary to the trends observed in the normal faulting scenario, the footing settlement and rotation estimated by the coupled and decoupled methodology are quite different. Initially (i.e. for low values of faulting dislocations) both systems rotate clockwise, but soon after the decoupled system starts rotating backwards, yielding an almost zero rotation at $\delta/\delta max \approx 0.3$. At this point the bridge pier fails and the footing is practically enforced to follow the soil deformation (rotation to the right). The snapshots of Fig. 11(b) illustratively explain the aforementioned response. Observe that the rupture of the decoupled system outcrops just beneath its right corner, provoking a counterclockwise rotation. On the other hand, when the coupled problem is considered, the main rupture is deviated away from the footing edge to the right, resulting in a clockwise rotation of the footing.

By just observing the footing rotations, it would be reasonable to expect that coupled system that experiences much higher rotation, would fail first. Yet, this is not the case. Both methodologies predict bending failure at the same level of imposed fault dislocations δ/δ_{max}, as shown in Fig. 12(a). Note that at that exact instant the coupled system presents negative drift values, caused by 'to-the-right' displacement of the deck. The latter induces positive curvature at the base of the pier that are partially cancelling the negative curvature produced by the footing rotation. A schematic representation of the aforementioned argumentation is shown in Fig. 12(c).

The distribution of bending moments across the deck of bridge, for imposed fault dislocation (δ/δ_{max} = 0.10), is presented in Fig. 13(a), while in Fig. 13(b) a comparison

between the coupled and decoupled system in terms of bending moments across the deck (for the same level of faulting) is presented. The differences of the two systems are very pronounced. The simplified decoupled methodology yields significantly higher bending moments (i.e. by a factor of 2). The reason why this happens, has already analyzed for the case of normal faulting.

Location 2: s/B = 0.46

For the second investigated faulting scenario the bending stress at the top and base of the two piers are portrayed in Fig. 14(a & d). Referring to the moment at the pier-base, the decoupled system is again driven first to failure, although the two systems at that exact instant are experiencing identical footing rotations. As vividly explained previously, in this case also, the kinematic loading applied at the superstructure (i.e. the horizontal movement at the left abutment), induces an opposite (favorable) curvature on the pier that prevents the ultimate bending failure.

Interestingly enough, the evolution of bending moment at the pier-base of the coupled system follows an abnormal pattern: the moment is peaking for fault level equal to δ/δ_{max} = 0.24 (Area 1), reduces for bedrock dislocations between δ/δ_{max} = 0.24 - 0.35 (Area 2) and continues increasing until reaching the ultimate value of M_{max} = 0.13 kNm at δ/δ_{max} = 0.5 (Area 3). To explain this behavior, we will attempt to separate the effects of the two competitive curvature-inducing mechanisms as the bedrock dislocation progresses: the footing rotation and the horizontal dislocation of the abutments that provokes pier drift, Fig. 14(b & c). Initially (Area 1), the foundation under the action of the main fault-rupture rotates considerably, while the top of the pier practically remains still (almost zero drift). This footing rotation provokes negative curvature and thus negative bending on the pier. As the coupled system enters Area 2, the foundation starts rotating backwards, the curvature decreases and so does the Bending Moment (in absolute terms). In Area 3 the pier drift attains positive values that in turn generate negative curvature and negative Moment. This continues until δ/δ_{max} = 0.55, the instant at which the pier capacity has been reached.

For this faulting case, an interesting behavior (in terms of footing displacements) may also be observed. Up to imposed dislocation level of δ/δ_{max} = 0.3, the two systems (coupled and

decoupled) behave in a similar manner: both footings accumulate almost identical settlements and rotations. Beyond this point, the system response changes drastically. The footing of the coupled system starts rotating backwards - yet maintaining a constant rate of settlement accumulation- while the exact opposite holds for the footing of the de-coupled system.

In order to gain insight on this response, Fig. 15(b & c) presents a set of deformed snapshots at two distinctive bedrock dislocations (δ/δ_{max} = 0.3 and δ/δ_{max} = 0.6). The readers are encouraged to observe the two ruptures interacting with the footing: a main rupture appearing near the footing right edge and a secondary rupture just behind the footing (evident for δ/δ_{max} = 0.6).

Clearly, the main rupture dominates the response for bedrock dislocations lower than δ/δ_{max} = 0.30. Yet for higher dislocation values the pattern get more complex. On the coupled system plastic strains keep accumulating along the main rupture, while in the decoupled system the secondary rupture is gaining ground. [Note that the intensity of plastic deformations in the main rupture remains practically unchanged from δ/δ_{max} = 0.30 to 0.60]. The latter forms a graben type deformation beneath the footing (of the coupled system) which restrains any additional clockwise foundation rotation (the footing tends to rotate towards the opposite side).

The distribution of bending moments across the deck of bridge for a fault dislocation δ/δ_{max} = 0.20 is presented in Fig. 17(a), while in Fig. 17(b) a comparison between the coupled and decoupled system in terms of bending moments across the deck (for the same level of faulting) is presented. The response of two systems, for the exact fault level, is identical. The cause of that is the equal settlement and rotation of decoupled with coupled footing, for the exact fault level, that is used as input fault dislocation on basis of decoupled detailed bridge model.

7. Some Insights on the fault-bridge interaction

Effect of Abutments

In this part of the study the effect of abutments on the response of bridge is investigated. Fig. 18(a) compares the bending stress for the two bridge piers. Evidently, the bending response of the two systems is completely different. The bridge with bearings leads the pier to failure, while the bending moment on the pier of the simply-supported system reaches a maximum value that is lower than the column capacity. Interestingly, this maximum value remain constant although the pier keeps rotating under the fault action. Yet this foundation rotation does not transmit bending stress on the pier column.

To elucidate further this peculiar response, in Fig 19 we have de-composed the bridge response into two separate mechanism: a deformation mechanism induced by the horizontal (to the right) movement of the fault, and a second one provoked by the vertical fault movement. Evidently, since the bridge deck is free to move horizontally, the first mechanism doesn't induce any stressing on the bridge. In the second mechanism however, the pier of simply-supported system is basically stressed due to the differential vertical movements of the left abutment ($u_{,2,FF}$) and the pier footing (u_2). This differential movement is translated to deck rotation and constant bending curvature along the pier. For the given M-k, the induced curvature of k=0.11 correspond to M=0.1 kNm. As long as the ratio of $u_{,2,FF}$ and u_2 remains constant the pier does not accumulate further stressing. Note that this is the maximum bending moment that may be developed to this bridge system.

Fig. 20(b) illustrates the distribution of soil stresses at the footing base at the instant of maximum moment. Observe the triangular distribution of soil pressures: the soil reaction in the right part of the foundation is zeroed, while increased stresses are concentrated on the left part. Naturally, the summation of soil pressure results in overturning moment of M=0.1 kNm that equals the developed Moment on the pier base.

8. Conclusions

This paper presents a numerical coupled methodology to analyze the response of bridges against large tectonic deformation. The numerical results have been systematically compared to those produced by applying the decoupled methodology suggested by *Anastasopoulos et al. 2008* and interesting conclusion have been derived. The conclusion derived apply to rigid bridge systems founded on surface are:

1. The design of bridges against tectonic deformation is quite feasible with proper design. The method of analysis presented by *Anastasopoulos et al. 2008* may form the basis for future Code provisions and requirements on the subject.
2. This efficiency of the decoupled methodology relies upon the accurate prediction of settlements and rotations at the bridge footings. The predictions were found to be more accurate for normal than for reverse faulting.
3. The rupture path is strongly affected by the presence of the superstructure. The emerging fault rupture is not only diverted, but may also be subjected to bifurcation and diffusion.
4. The bridge system with simple supports on its abutments, leads to lower pier bending stress than original problem. Therefore it is vital to correctly account the abutment stiffness in the experimental set-up, in order to correctly simulate the bridge-fault interaction problem.

9. References

Anastasopoulos I, Gazetas G, Bransby MF, Davies MCR, El NahasA(2007) Fault rupture propagation through sand: finite element analysis and validation through centrifuge experiments. J Geotech Geoenviron Eng ASCE 133(8):943–958

Anastasopoulos I, Gazetas G, Drosos V, Georgarakos T, Kourkoulis R (2008) Design of bridges against large tectonic deformation. Earthq Eng Eng Vib 7:345–368

Anastasopoulos I, Gazetas G, Bransby MF, Davies MCR, El Nahas A (2009) Normal fault rupture interaction with strip foundations. J Geotech Geoenviron Eng ASCE 135(3):359–370

Anastasopoulos I, Georgarakos T, Georgiannou V, Drosos V, Kourkoulis R (2010) Seismic performance of bar-mat reinforced-soil retaining wall: shaking table testing versus numerical analysis with modified kinematic hardening constitutive model. Soil Dyn Earthq Eng 30(10):1089–1105

Bolton MD (1986) The strength and dilatancy of sands. Geotechnique 36(1):65–78

Bransby MF, Davies MCR, El Nahas A, Nagaoka S (2008) Centrifuge modelling of normal fault-foundation interaction. Bull Earthq Eng 6(4):585–605

Bray JD, Seed RB, Cluff LS, Seed HB (1994) Analysis of earthquake fault rupture propagation through cohesive soil. J Geotech Eng 120(3):562–580

Bray JD, Seed RB, Cluff LS, Seed HB (1994) Earthquake fault rupture propagation through soil. J Geotech Eng 120(3):543–561

Bray JD (2001) Developing mitigation measures for the hazards associated with earthquake surface fault rupture, A Workshop on Seismic fault-induced failures—Possible Remedies for Damage to Urban Facilities, Japan Society for the Promotion of Sciences, 55–79

Bray JD (2009) Designing buildings to accommodate earthquake surface fault rupture, improving the seismic performance of existing and other structures. ASCE, Reston, pp 1269–1280

Fadaee M, Anastasopoulos I, Gazetas G, Jafari MK, Kamalian M (2013) Soil bentonite wall protects foundation from thrust faulting: analyses and experiment. Earthq Eng Eng Vib 12(3):473–486

Gazetas G, Pecker A, Faccioli E, Paolucci R, Anastasopoulos I (2008) Design recommendations for fault–foundation interaction. Bull Earthq Eng 6(4):677–687

Gazetas G, Zarzouras O, Drosos V, Anastasopoulos I (2015) Bridge-Pier-Caisson foundations subjected to normal and thrust faulting: physical experiments versus numerical analysis. Meccanica (2015) 50:341–354

Loli M, Anastasopoulos I, Bransby MF, Waqas A, Gazetas G (2011) Caisson foundations subjected to reverse fault rupture: centrifuge testing and numerical analysis. J Geotechn Geoenviron Eng ASCE 137(10):914–925

Loukidis D, Bouckovalas G, Papadimitriou AG (2009) Analysis of fault rupture propagation through uniform soil cover. Soil Dyn Earthq Eng 29(11–12):1389–1404

Muir Wood D (2004) Geotechnical modelling. Spon Press, London and New York

Oettle NK, Bray JD (2013) Geotechnical mitigation strategies for earthquake surface fault rupture. Geotechn Geoenviron Eng 139(11):1864–1874

Paolucci R, Yilmaz MT (2008) Simplified theoretical approaches to earthquake fault rupture–shallow foundation interaction. Bull Earthq Eng 6(4):629–644

Annex of Charts

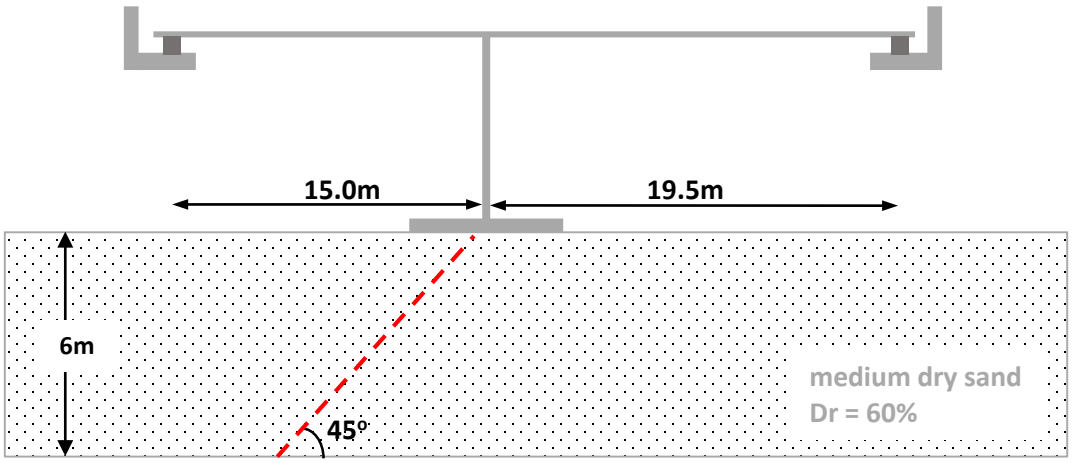

Figure 1. Sketch of the studied problem indicating the key parameters and dimensions at prototype scale. Dimensions apply to both **normal** and **thrust** rupturing faulting.

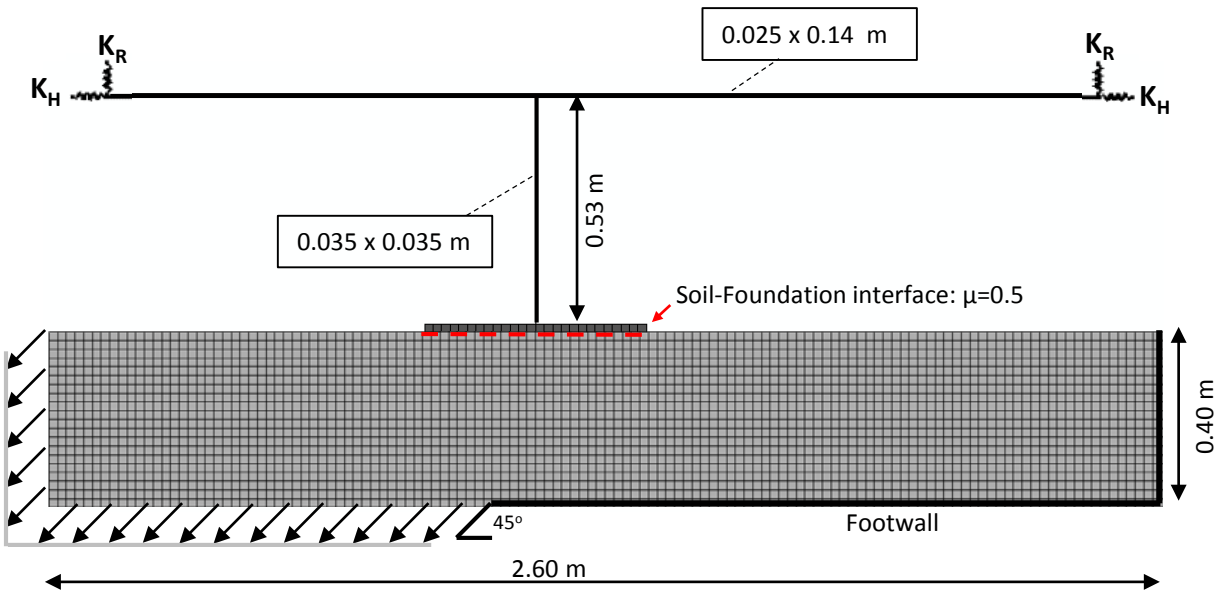

Figure 2. View of the 2D Finite Element model, along with key model dimensions and boundary conditions.

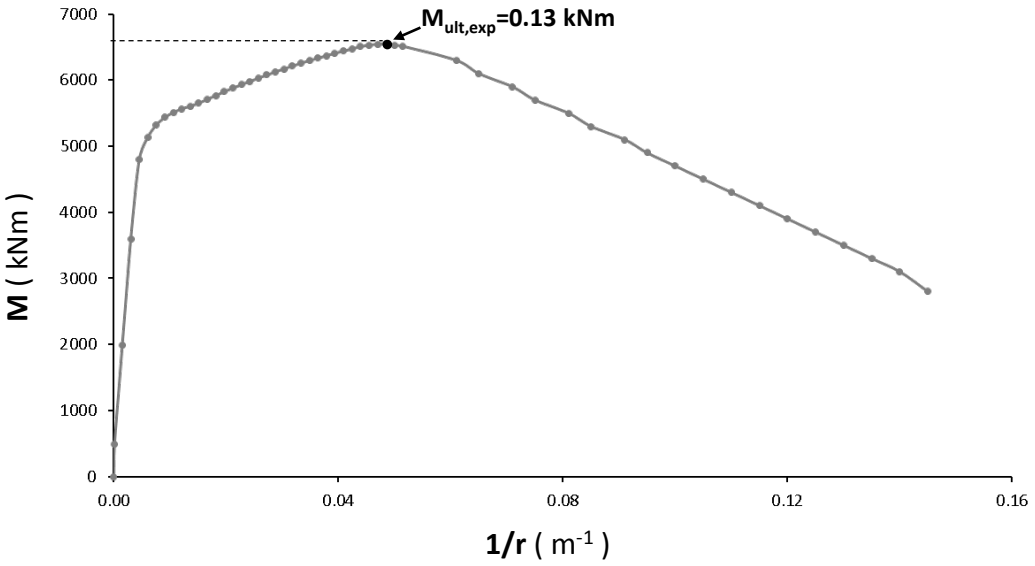

Figure 3. The Non-linear Bending response of the RC bridge pier (prototype scale), in terms of curvature (**1/r**) – moment (**M**).

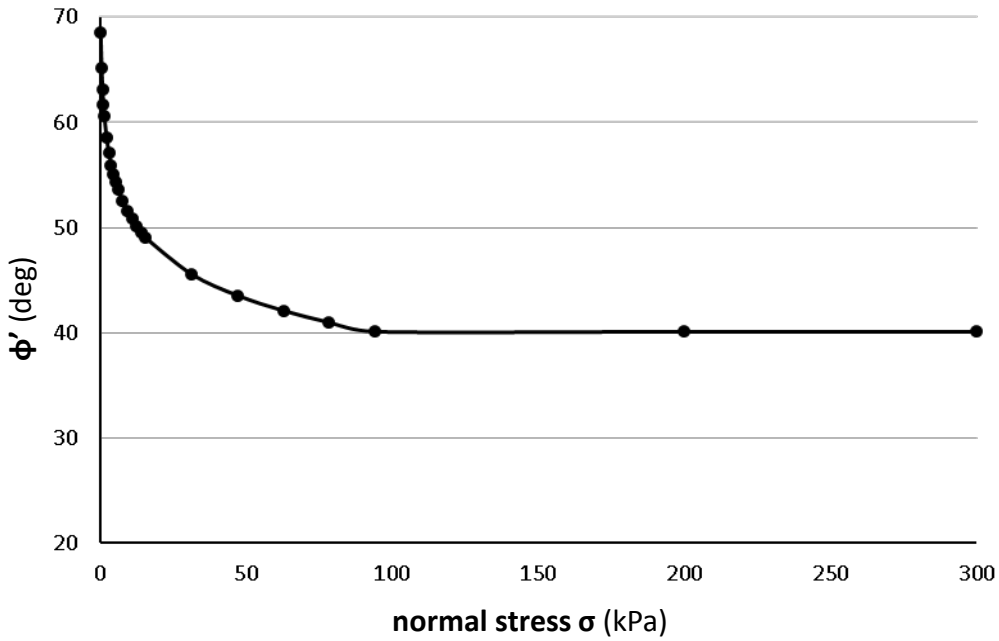

Figure 4. Direct shear results for the Longstone sand: mobilized friction angle as a function of stress level.

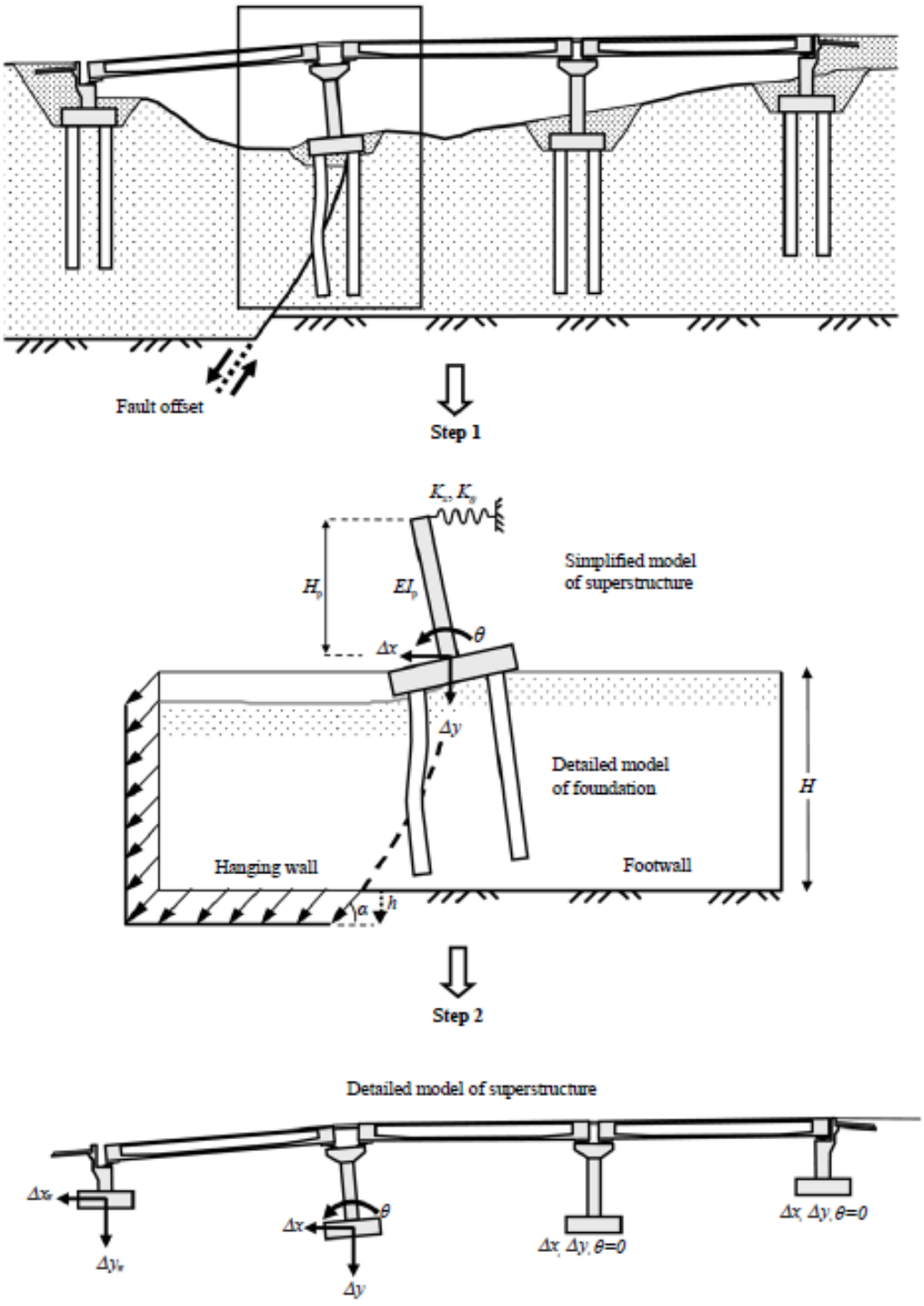

Figure 5. The decoupled Methodology proposed by *Anastasopoulos et al (2008)* : the analysis of the soil–structure system subjected to faulting-induced deformation is conducted in two steps. In Step 1, we analyze the response of a single bridge pier subjected to fault rupture deformation. In Step 2, the detailed model of the superstructure is subjected to the computed displacements and rotations of Step 1.

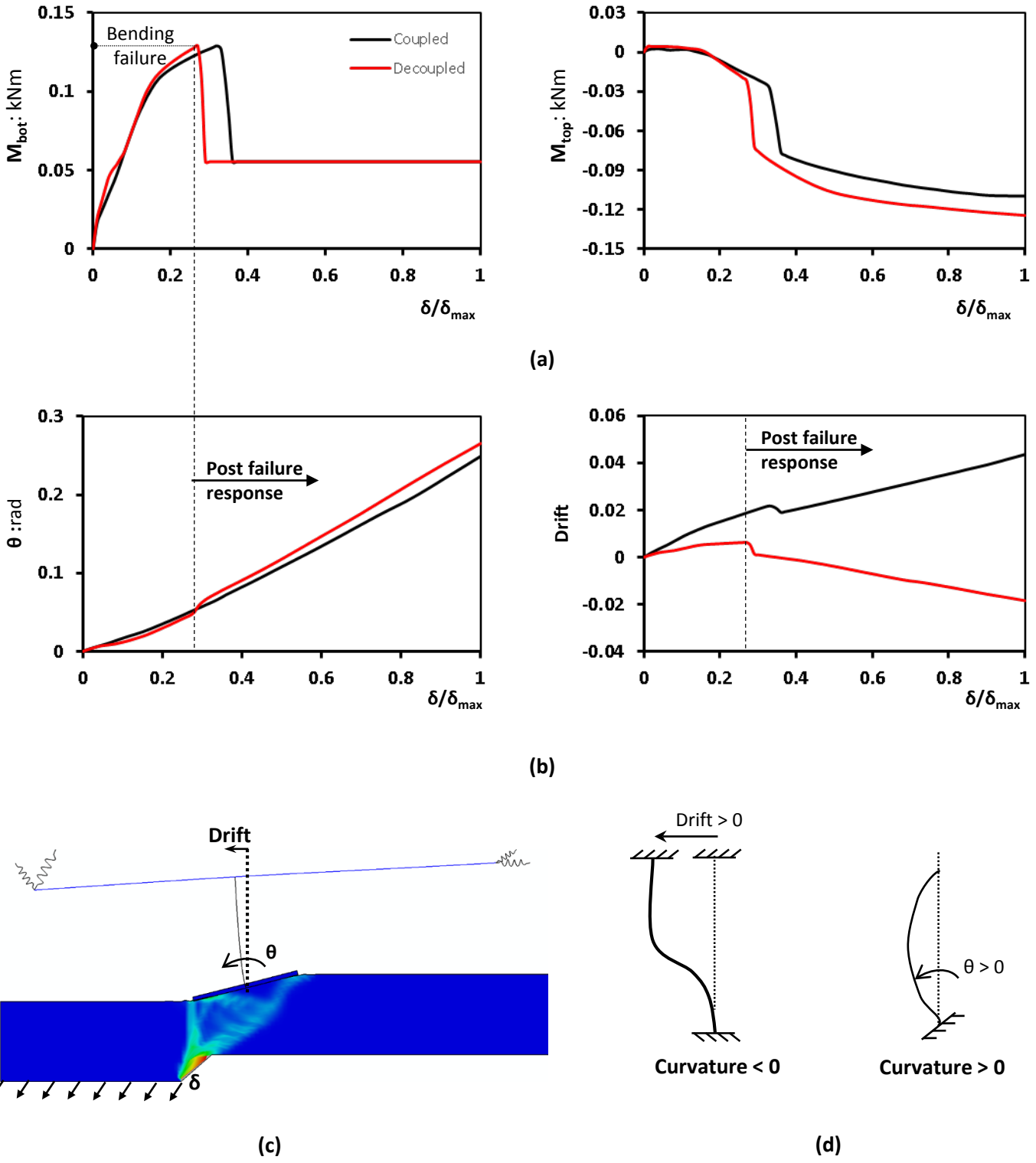

Figure 6. Bridge subjected to normal faulting (δ_{max}=-0.1m). Results are presented in terms of : **(a)** bending moments on the top (M_{top}) and bottom (M_{bot}) of the pier; and **(b)** rotation of footing (θ) and drift ratio of pier. **(c)** View of the deformed coupled system; **(d)** kinematics responsible fro the bending stressing on the pier of the coupled system.

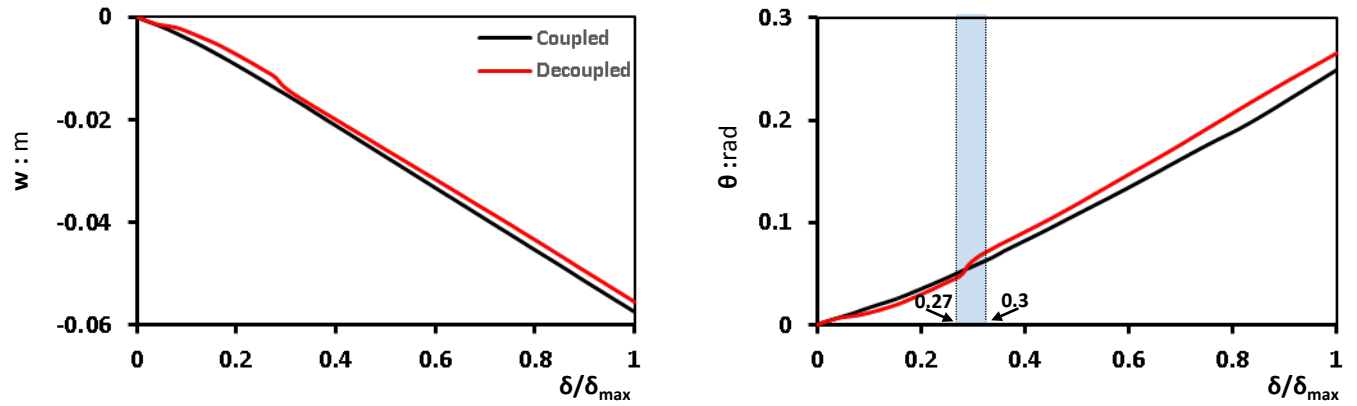

(a)

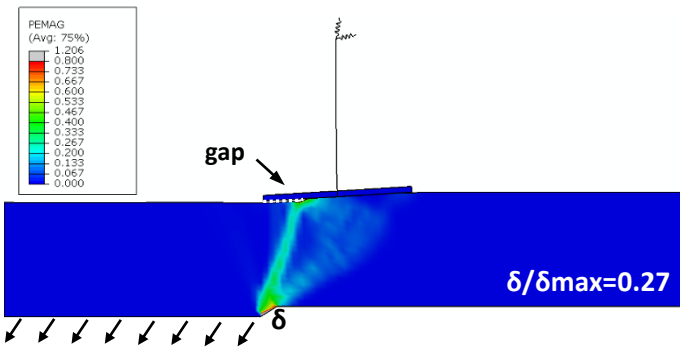

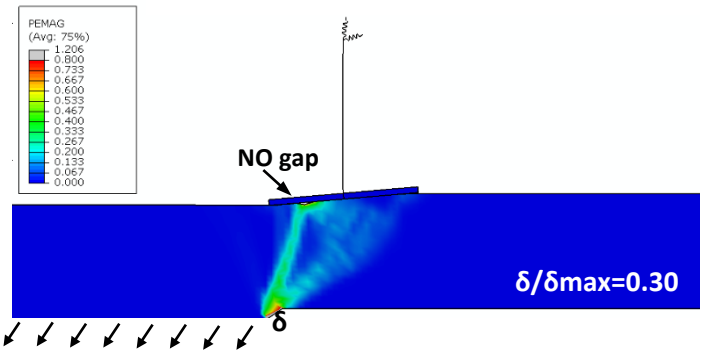

(b)

Figure 7. Bridge subjected to normal faulting (δ_{max}=-0.1m) : **(a)** settlement (w) and rotation (θ) at the footing and **(b)** snapshots of the deformed decoupled problem at two distinctive instants.

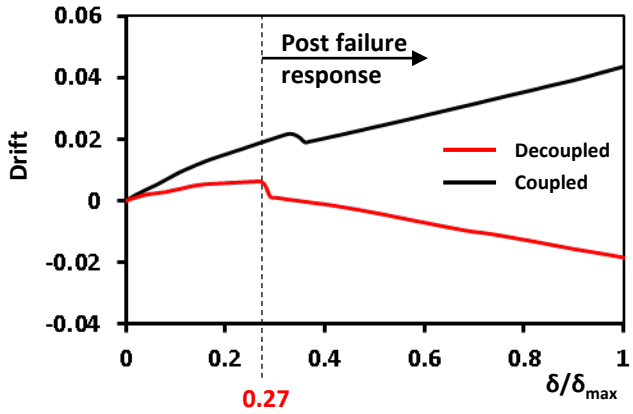

(a)

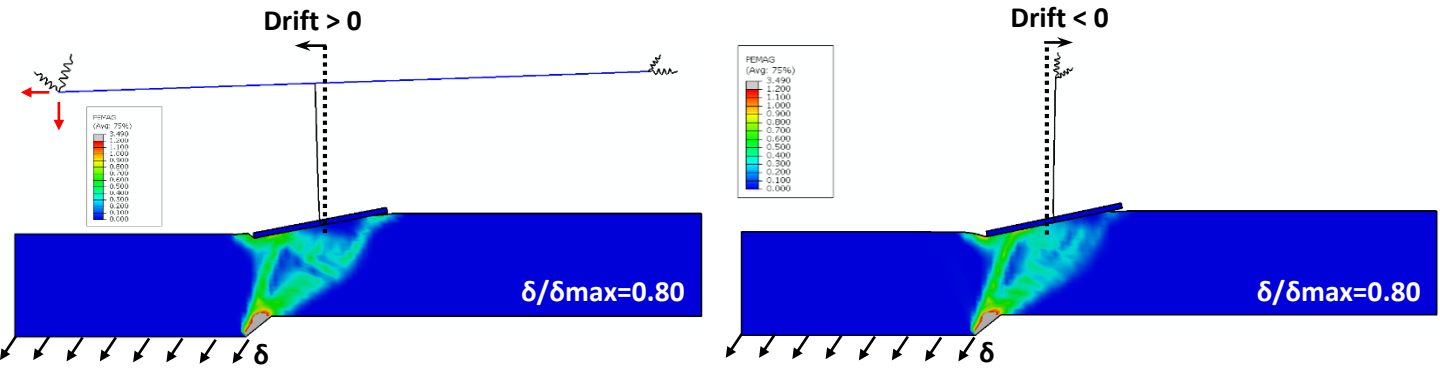

(b)

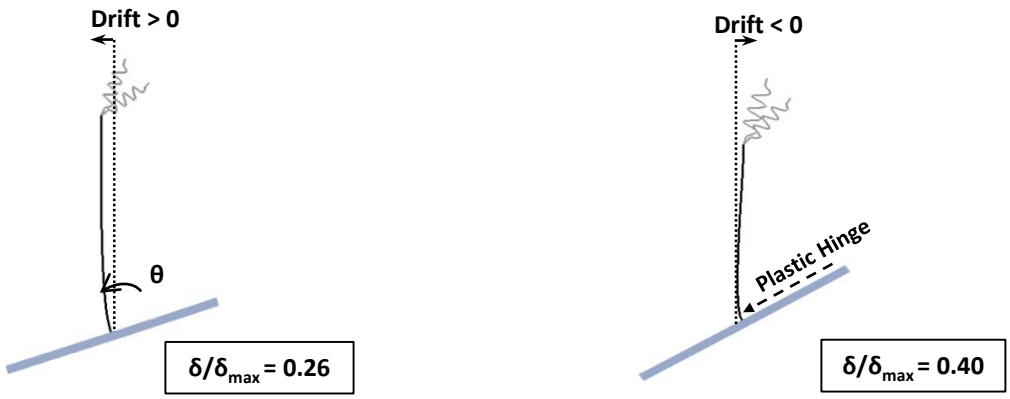

(c)

Figure 8. Bridge subjected to normal faulting analyzed (δ_{max}=-0.1m). Results are presented in terms of **(a)** drift ratio of the pier and **(b)** deformation snapshots superimposed with plastic deformation contours. **(c)** View of the deformed shape of decoupled system-pier, clarifying the differences of drift ratio before and after the development of plastic hinge (at instant δ/δ_{max} = 0.27).

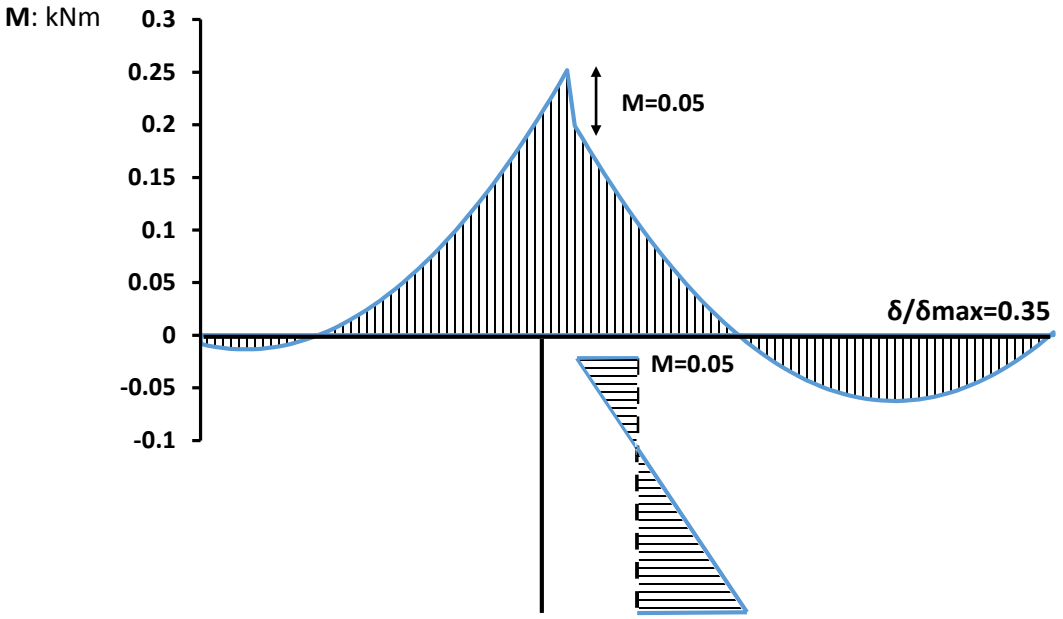

(a)

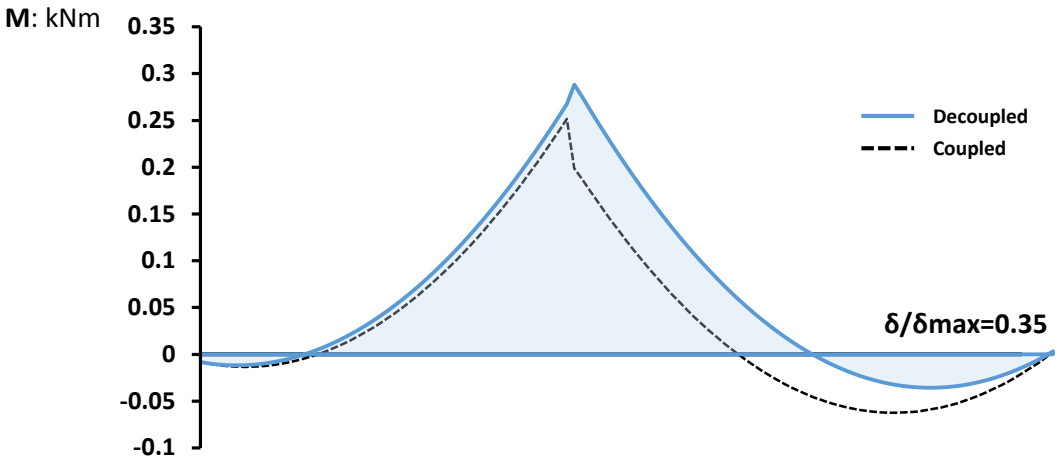

(b)

Figure 9. (a) Bending Moment distribution of the coupled system when subjected to normal faulting of δ/δ_{max} = 0.35 (δ_{max}=-0.1m); and **(b)** bending moment distribution along the bridge deck.

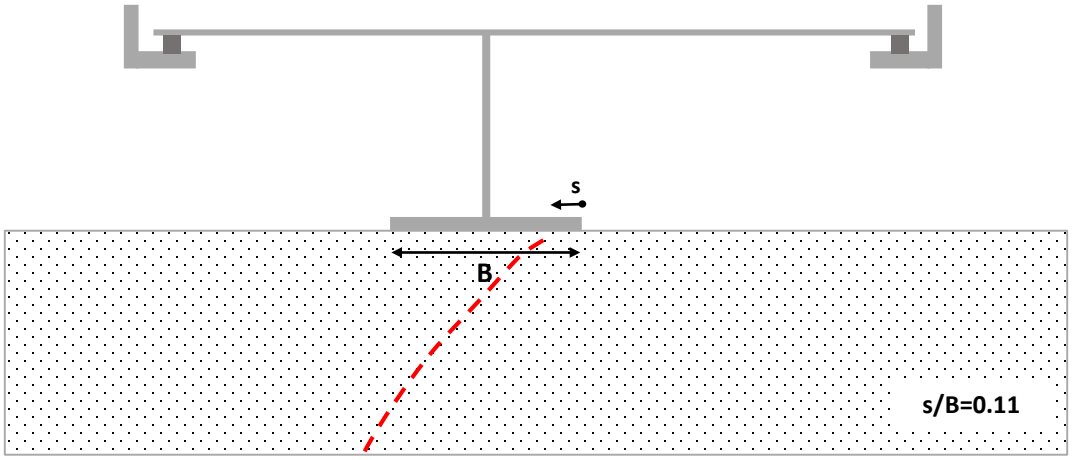

(a)

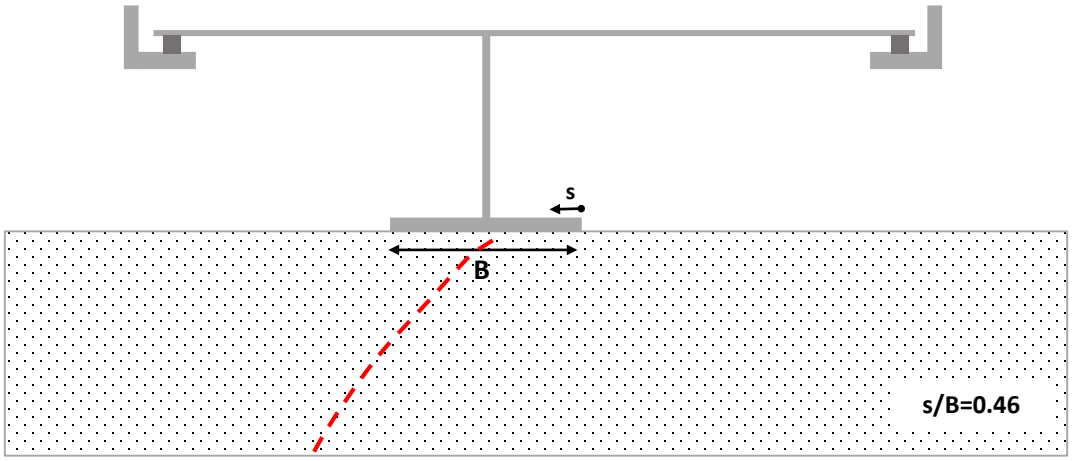

(b)

Figure 10. Bridge subjected to reverse faulting : **(a)** *free-field* rupture crosses the right corner of bridge footing (s/B=0.11) and **(b)** *free-field* rupture crosses the center of bridge footing (s/B=0.46).

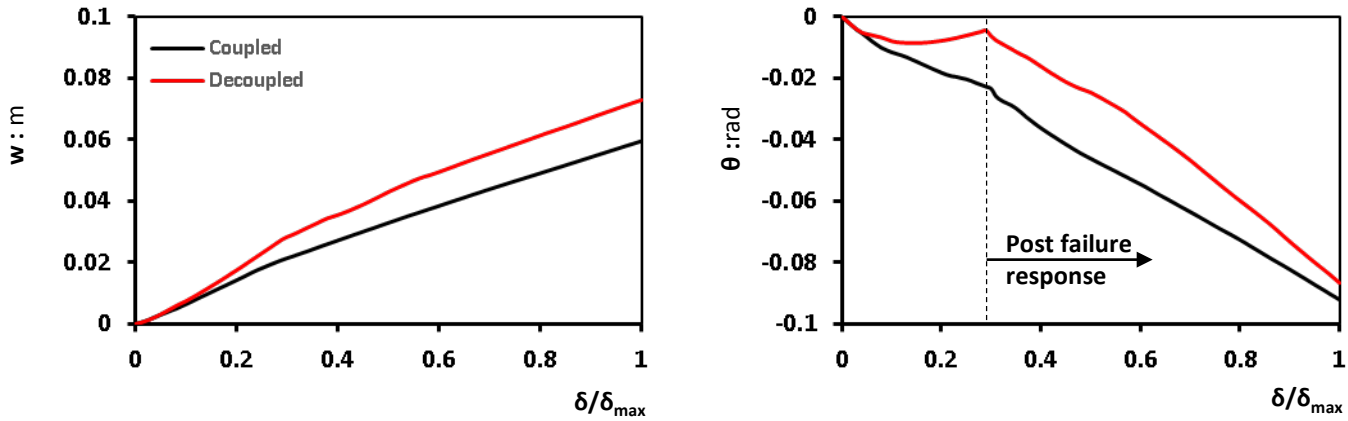

(a)

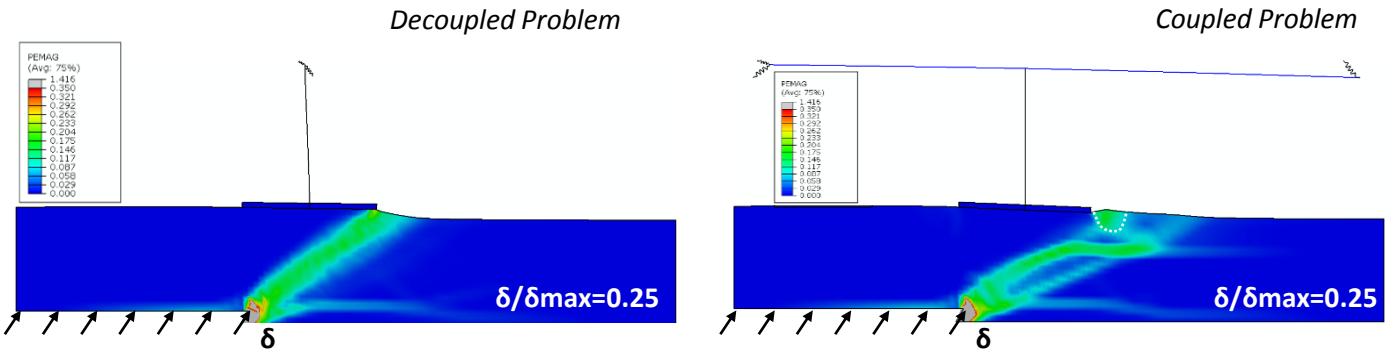

(b)

Figure 11. Bridge subjected to reverse faulting at s/B=0.11 (δ_{max}=0.1m): **(a)** settlement (w) and rotation (θ) at the footing and **(b)** snapshots of two systems at fault dislocation level δ/δ_{max} = 0.25.

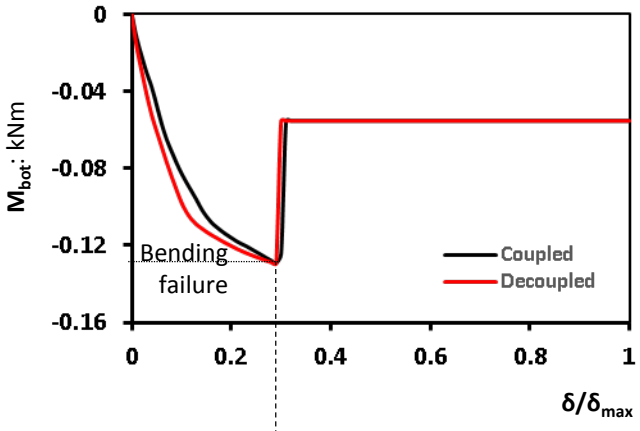

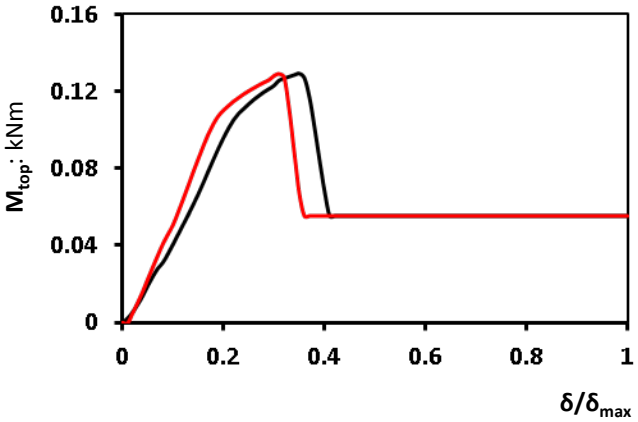

(a)

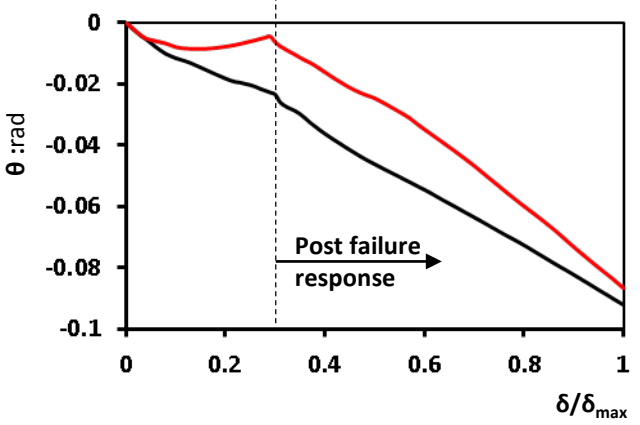

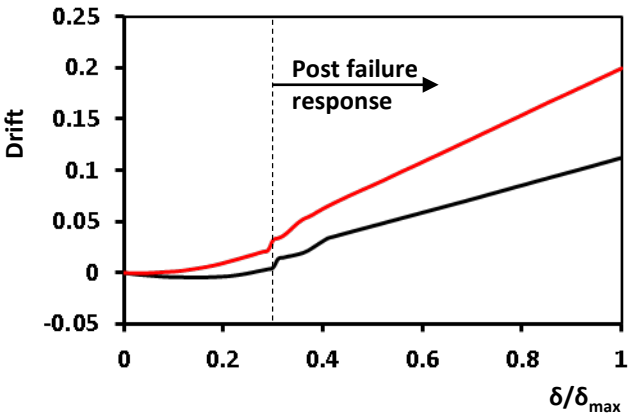

(b)

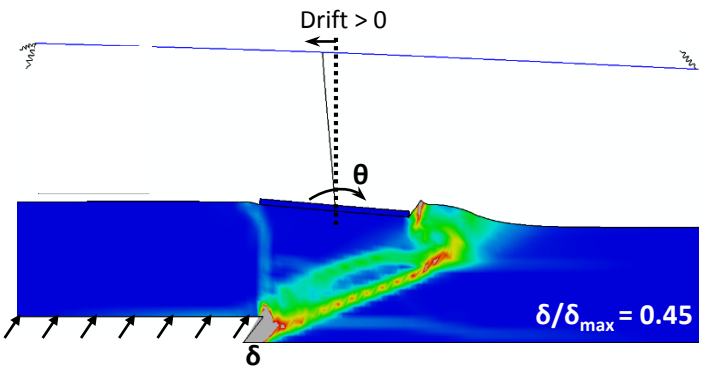

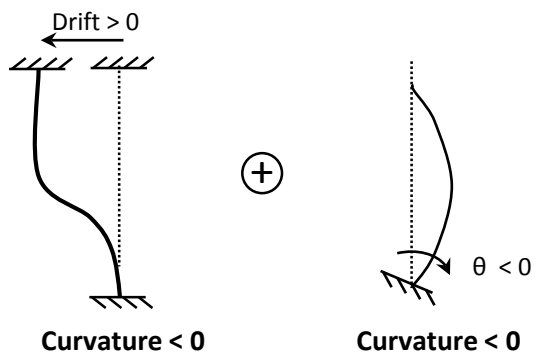

(c) (d)

Figure 12. Bridge subjected to reverse faulting (δ_{max}=0.1m). Results are presented in terms of : **(a)** bending moments on the top (M_{top}) and bottom (M_{bot}) of the pier; and **(b)** rotation of footing (θ) and drift ratio of pier; **(c)** view of the deformed coupled system at δ/δ_{max}=0.45; **(d)** kinematics responsible fro the bending stressing on the pier of the coupled system.

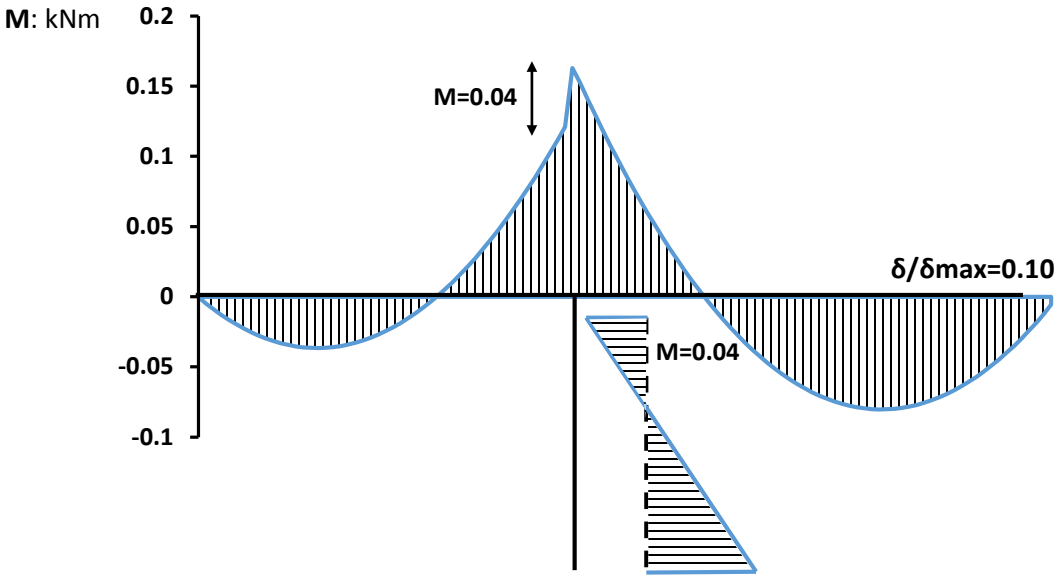

(a)

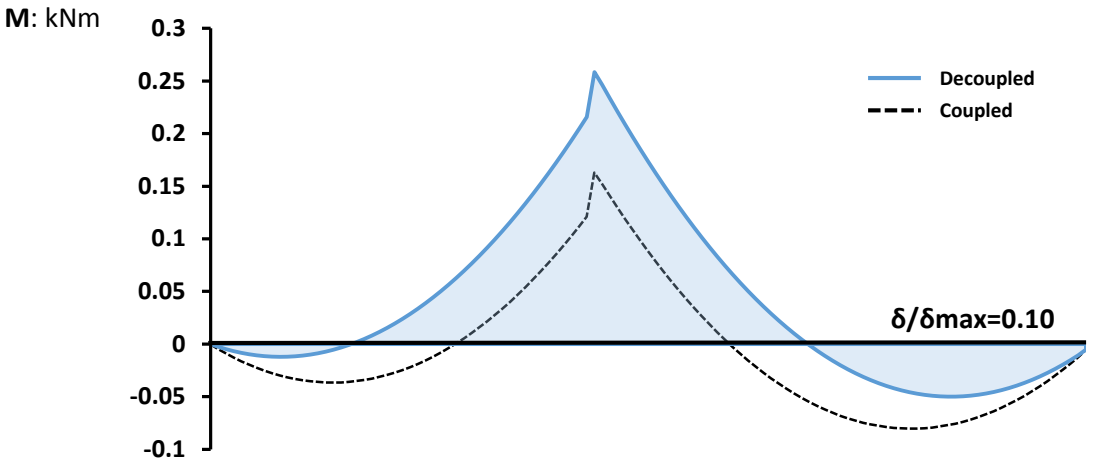

(b)

Figure 13. (a) Bending Stressing of the bridge (calculated by means of a coupled analysis) at reverse faulting δ/δ_{max} = 0.10 (δ_{max}=0.1m); **(b)** bending moments along the bridge deck for both systems.

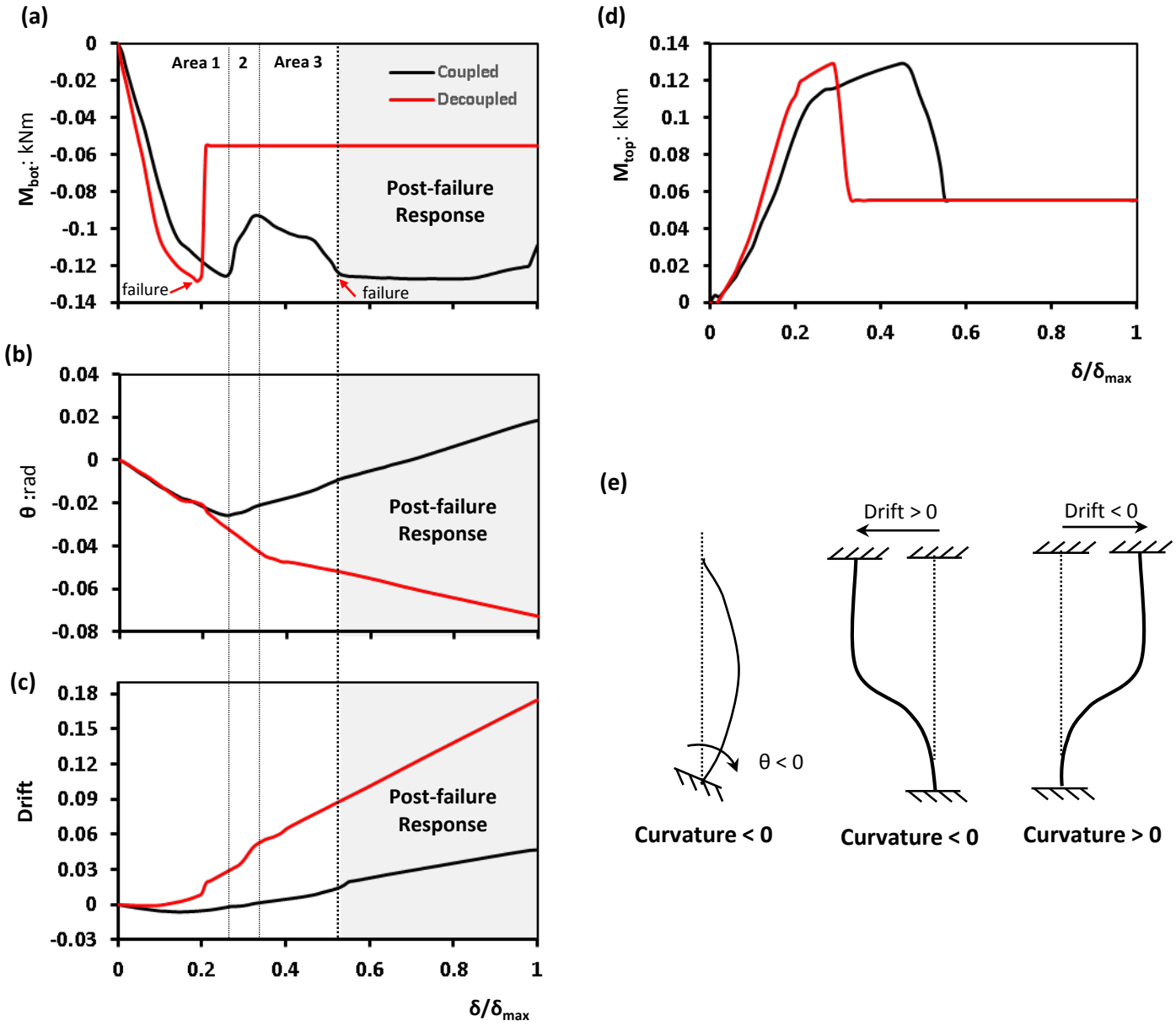

Figure 14. Bridge subjected to reverse faulting at s/B=0.46 (δ_{max}=0.1m). Results are presented in terms of : **(a)** bending moments on the bottom (M_{bot}) of pier; **(b)** rotation (θ) of footing; **(c)** drift ratio of pier; and **(d)** bending moments on top (M_{top}) of the pier. **(e)** Defromation pattern nomenclature.

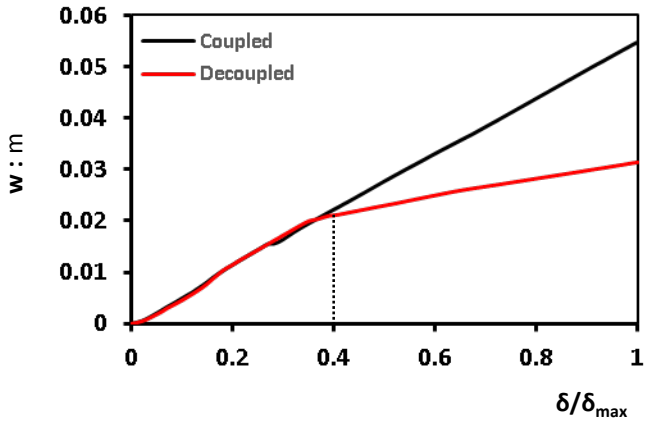

(a)

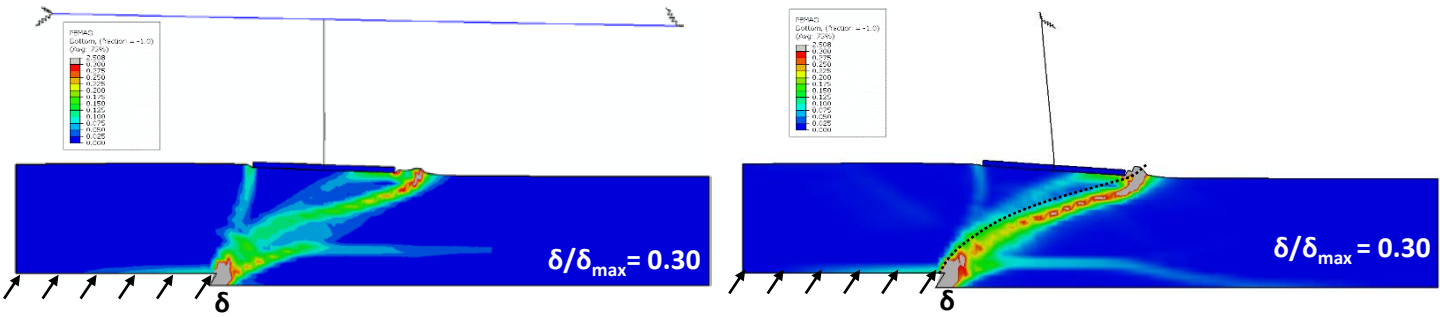

(b)

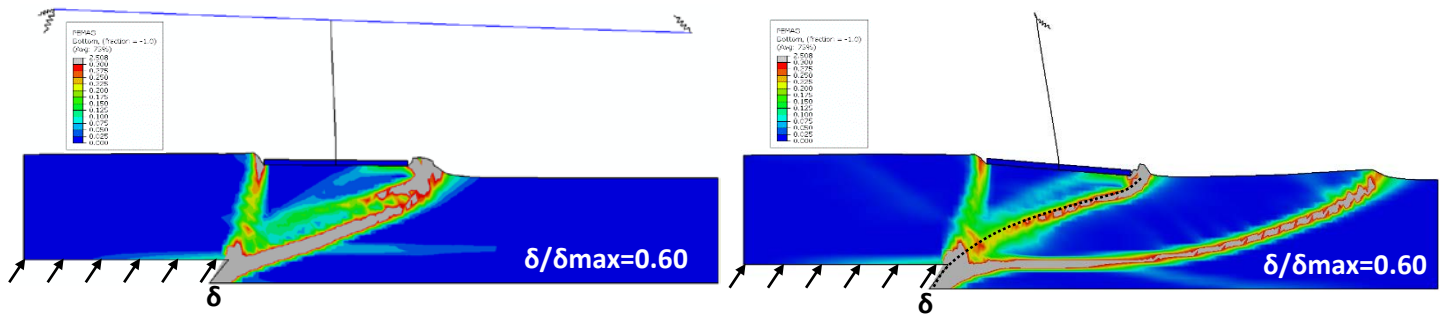

(c)

Figure 15. Bridge subjected to reverse faulting (δ_{max}=0.1m). **(a)** Footing settlement as derived by the coupled and the decoupled methodoloigy. Deformation snapshots superimposed with plastic deformation contours for both systems at **(b)** δ/δ_{max}= 0.30 and **(c)** δ/δ_{max}= 0.60.

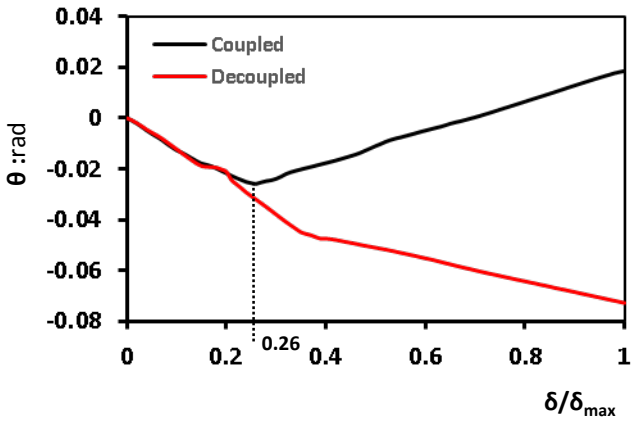

(a)

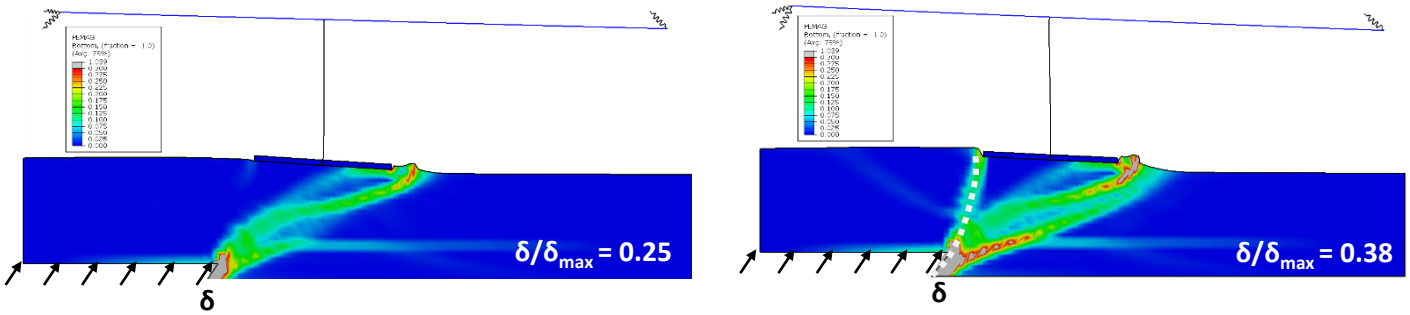

(b)

Figure 16. Bridge subjected to reverse faulting (δ_{max}=0.1m): **(a)** foundation rotation (θ) and **(b)** snapshots of the coupled system at two distinctive bedrock dislocations δ/δ_{max} = 0.25 and 0.38.

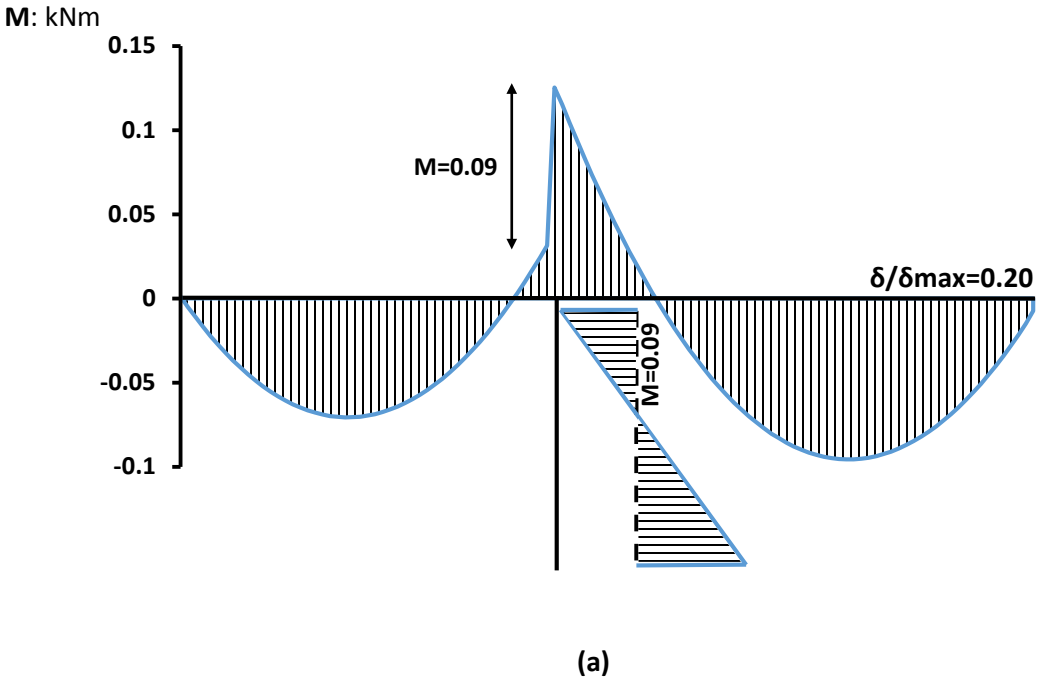

(a)

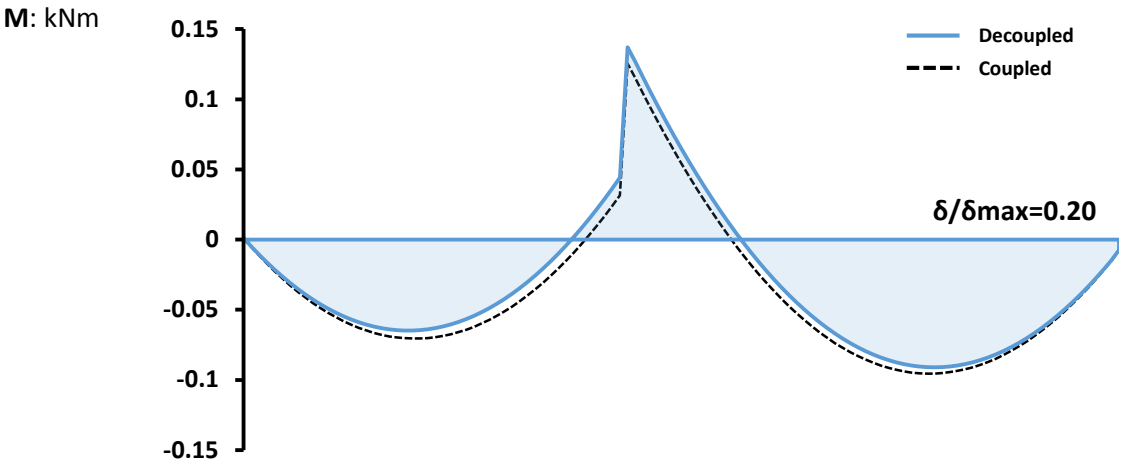

(b)

Figure 17. (a) Bending Stressing of the bridge (calculated by means of a coupled analysis) at reverse faulting of δ/δ_{max} = 0.20 (δ_{max}=0.1m); and **(b)** bending moments along the bridge deck for both systems.

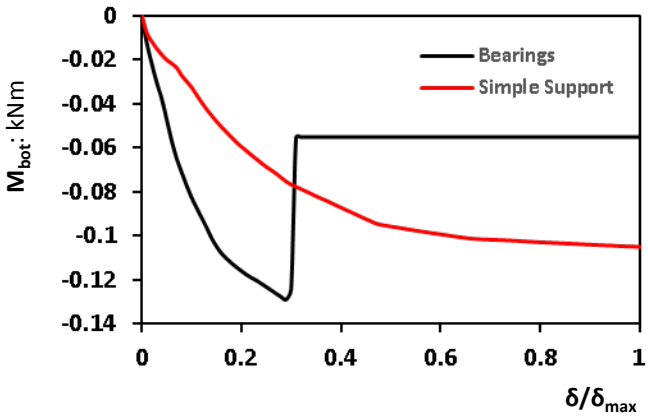

(a)

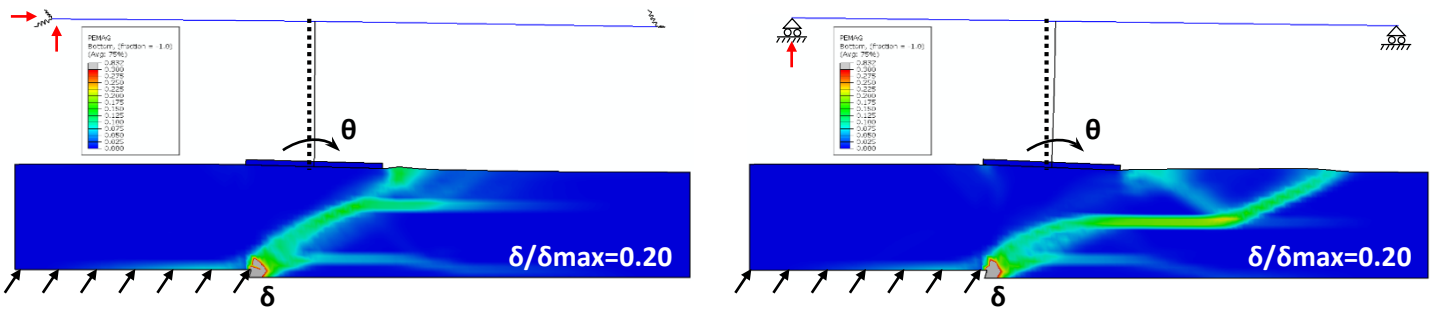

(b)

Figure 18. Bridge subjected to reverse faulting analyzed with bearings and simple supports on its abutments: **(a)** bending moments on the bottom (M_{bot}) of pier; **(b)** snapshots of two systems at the same fault dislocation level (δ/δ_{max} = 0.20).

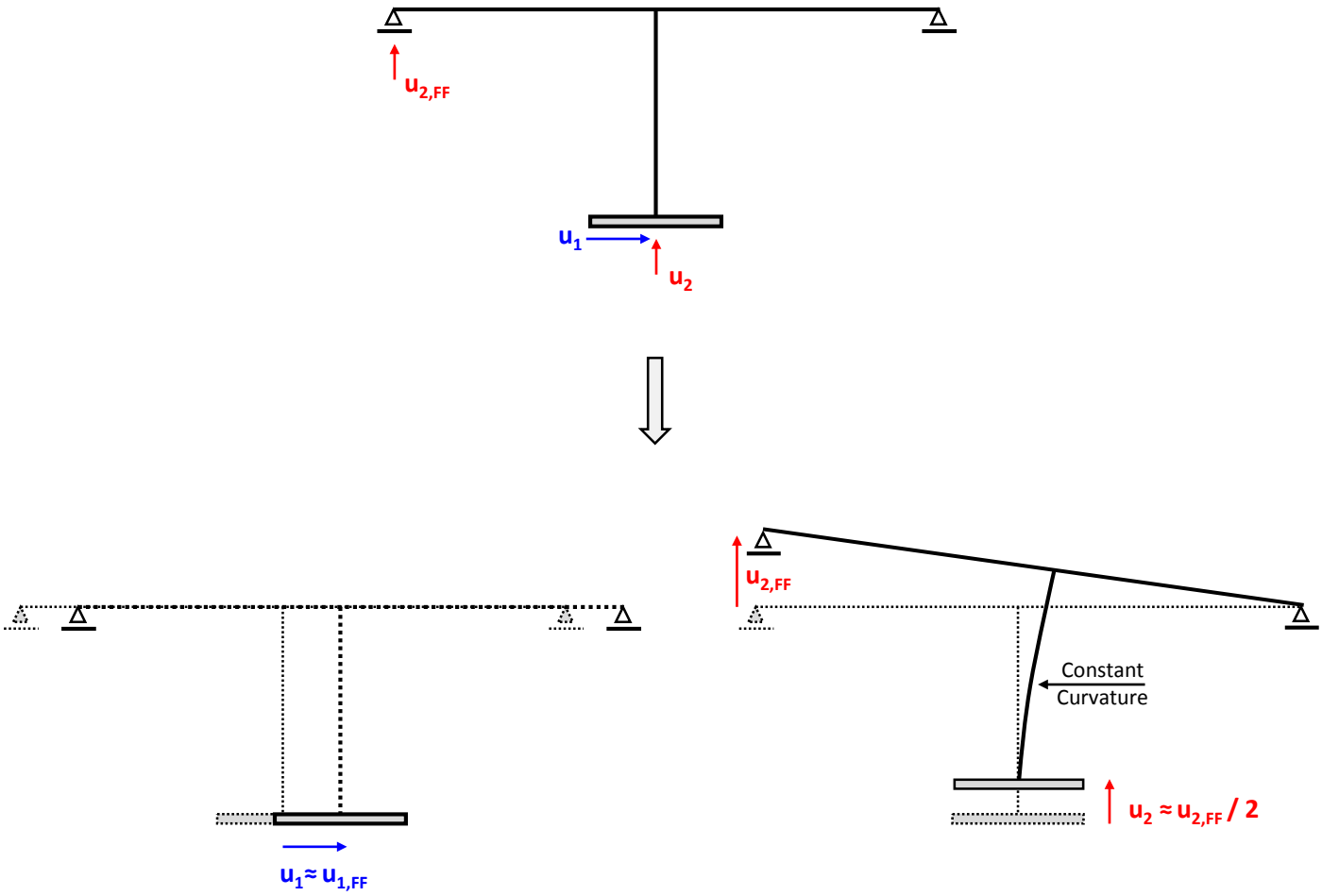

Figure 19. Simply-supported bridge subjected to reverse faulting: schematic representation of the stressing mechanism.

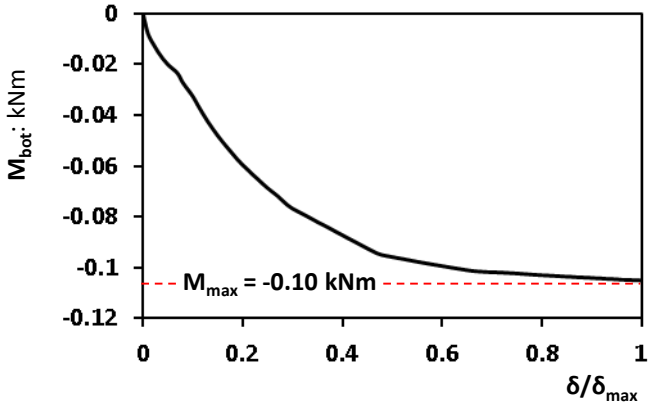

(a)

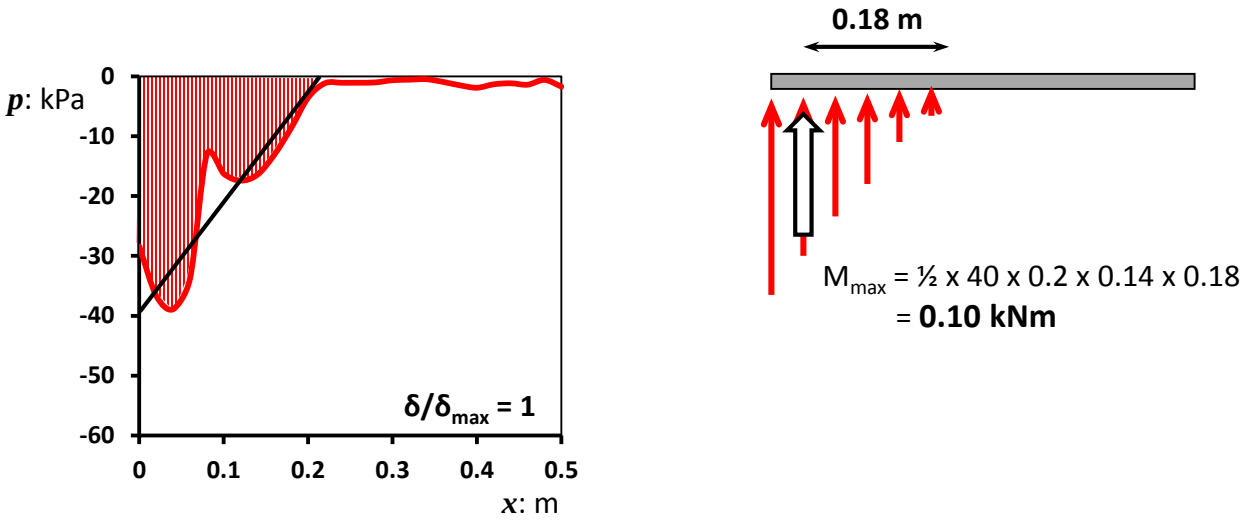

(b)

Figure 20. Simply supported bridge subjected to reverse faulting : **(a)** developed bending moments on the pier base (M_{bot}) ; **(b)** distribution of vertical soil stresses just beneath the footing at fault dislocation δ/δ_{max} = 1(i.e. when the bending moment of pier is maximum).